Surface & Coatings Technology 397 (2020) 125990

Contents lists available at ScienceDirect

Surface & Coatings Technology

journal homepage: www.elsevier.com/locate/surfcoat

Tailoring residual stresses in CrN_x films on alumina and silicon deposited by high-power impulse magnetron sputtering

Robin Elo*, Staffan Jacobson, Tomas Kubart

Uppsala University, Box 534, SE-75121 Uppsala, Sweden

ARTICLE INFO

Keywords:
Chromium nitride
Magnetron sputtering
Residual stress
Scratch resistance
HiPIMS

ABSTRACT

Chromium nitride films, deposited using reactive magnetron sputtering, were optimised for wear resistance. The performance was measured by scratch resistance and optimised by tailoring the residual stresses. The depositions were carried out with either direct current magnetron sputtering (DCMS) or high-power impulse magnetron sputtering (HiPIMS), and with varying substrate bias and nitrogen gas flow. With DCMS, all films remained under tensile stresses and exhibited poor performance in scratch testing. Although the tensile stresses could be reduced by increasing the nitrogen flow, compressive stresses could only be induced when employing HiPIMS. Substrate bias had a strong effect in HiPIMS in contrast to the DCMS. The effect of the substrate bias in HiPIMS can be explained by the high ionisation of the flux of film forming species. In all cases, increased nitrogen flow favoured formation of CrN over Cr_2N. All films showed signs of limited adhesion, which was improved using a titanium interlayer. Cracking across the scratch could be completely avoided for films with lower tensile or compressive stresses, the latter also exhibiting the highest critical load. The results show that it is possible to increase the scratch resistance by tailoring the residual stresses, for which HiPIMS proved a very useful tool.

1. Introduction

Chromium nitride (CrN_x) is one of the most common ceramic coating materials. It has been used as a hard coating since the early 1980's and is well suited to be deposited by reactive sputtering [1]. Advantageous properties of CrN include relatively high wear resistance and high coefficient of friction (CoF) against steel and ceramics [2–4]. This combination is beneficial when a high grip in a contact is desired to avoid sliding, and the wear rate must be kept low.

CrN coatings might be beneficial also on hard ceramic materials, such as alumina. Although alumina is chemically inert and hard, self-mated alumina surfaces are sensitive to variations in humidity, which lead to variations in CoF and wear [5]. Coating one of the surfaces in an alumina/alumina couple with CrN may therefore make the CoF more stable, and the CoF against alumina has been reported to be relatively high [2,3].

Residual stresses are very important for the performance of coatings as the adhesion is of utmost importance. There is no single answer on how to optimise the adhesion; it is a combined product of interface strength, residual stresses, surface topography, and loads in the mechanical contact. In the case of CrN, the residual stresses are of extra interest since the film composition and sputtering conditions can heavily alter the stress level from high tensile to high compressive in the coating [6,7]. In magnetron sputtering, variation of the substrate bias is typically used to adjust the residual stresses. Higher substrate bias results in higher energy of the ions impinging on the substrate, which leads to ion implantation and thus generation of higher compressive stresses [8,9].

High-power impulse magnetron sputtering (HiPIMS) has been proven very useful for stress engineering in thin film technologies [10,11]. In this variant of magnetron sputtering, a standard magnetron sputtering cathode is operated in a pulsed mode at a low duty cycle and at a low frequency, to achieve a very high peak power. Thus, peak power densities of about 0.5–10 kW/cm^2 are achieved, which is two orders of magnitude higher than in standard sputtering [12]. This leads to significantly enhanced ionisation of the sputtered species, with beneficial consequences in the form of increased density, enhanced adhesion, or improved microstructure of the deposited coatings [13,14]. Another advantage of the HiPIMS technique is its compatibility with standard direct current magnetron sputtering (DCMS) hardware – the average discharge power is kept at values comparable to DCMS.

HiPIMS deposition of CrN has been investigated in a number of reports. In an early publication, Mayrhofer et al. [7] demonstrated hard CrN films and the effect of the ion to atom flux ratio on the film microstructure. Ehiasarian et al. [15] showed that the ion assistance in HiPIMS leads to a dense microstructure and thus improved corrosion

* Corresponding author.
E-mail address: robin.elo@angstrom.uu.se (R. Elo).

https://doi.org/10.1016/j.surfcoat.2020.125990
Received 29 January 2020; Received in revised form 28 May 2020; Accepted 31 May 2020
Available online 02 June 2020

resistance. The HiPIMS process offers means to tune the residual stresses in the film, although the deposition rate is typically lower than in DCMS [16,17]. Other studies analysed the relation between the processing conditions in different variants of HiPIMS and film microstructure [18–20]. Despite the intense research effort, the benefits of HiPIMS for material synthesis are still debated and the industrial uptake of HiPIMS is relatively slow. In this work, we show the impact of HiPIMS on the scratch resistance of CrN coatings deposited on alumina substrates. HiPIMS and DCMS reactive deposition of CrN_x is analysed and the relation between processing conditions, residual stresses, and the scratch behaviour is discussed.

2. Method and materials

Chromium nitride (CrN_x) was deposited using reactive magnetron sputtering on alumina and silicon substrates. All depositions were carried out in a Lesker CMS-18 ultra-high vacuum deposition system with a base pressure below 10^{-5} Pa. The system was equipped with four magnetron sputtering sources tilted with an angle of 16° in a co-sputtering configuration. The target-to-substrate distance was approximately 180 mm. For the experiments, two magnetron sources Torus 4 HV were used with planar circular targets, with a thickness of 6 mm and a diameter of 101 mm. Metal Ti (99.7% purity) and Cr (99.95%) targets were used. The depositions were performed in a mixture of Ar (99.9995%) and N_2 (99.9995%) at a constant deposition pressure of 0.5 Pa. The mass flow of Ar was kept constant at 50 sccm (standard cubic centimetre per minute) while the N_2 flow was either 20 or 30 sccm. The substrates were placed on a rotating substrate holder and biased during the deposition. The depositions were carried out in DCMS and HiPIMS modes of sputtering without intentional substrate heating. In both cases, the average discharge power was kept at 500 W. The HiPIMS sputtering power was delivered by a Melec SIPP 1000 pulsing unit supplied by an Advanced Energy Pinnacle DC generator. The average power was calculated from the instantaneous power, monitored using current and voltage transducers. A pulse on-time of 100 µs and a frequency of 500 Hz were used. The pulse power P_p is calculated from the energy per pulse as:

$$P_p = \frac{\int_0^{T_{on}} I * U \, dt}{T_{on}} \tag{1}$$

where T_{on} is the pulse on-time. DCMS depositions were carried out using an Advanced Energy Pinnacle+ power supply, operated in pulsed DC mode at a frequency of 50 kHz. In biased depositions, a pulsed bipolar DC bias (frequency of 250 kHz, 1.6 µs off time) was applied by another Pinnacle+ generator to the substrate.

Process parameters were varied to optimise the scratch resistance, specifically by tailoring the phases in and residual stress of the films. The variations in deposition conditions are summarised in Table 1. Metallic interlayers are often used as a mean to increase the adhesion to the substrate [3,21,22]. Preliminary results indicated that a Ti interlayer performed best, hence about 50 nm of Ti was used in all experiments.

The deposited films with a total thickness of about 800 nm were characterized with respect to structure, residual stress, and scratch resistance. The film thickness was controlled by deposition time and measured on cleaved cross sections by electron microscopy.

The film stresses were determined from the curvature they caused on the coated Si wafers. The Si substrates were 200 µm thick, with a size of about 20 by 20 mm. The curvature was measured by coherent scanning interferometry (CSI), using coherence of two light paths to find the local height of the surface. First, the whole surface was measured to find the centre of the curvature and then the central 6 by 6 mm area was analysed. The horizontal and vertical curvatures were used to estimate the film stresses in two directions, using Stoney's equation [23,24]. The presented value is the average of these:

$$\sigma_f = \frac{E_s * d_s^2}{6(1-\nu_s)} * \frac{1}{d_f} * \frac{1}{R} \tag{2}$$

where σ_f is the calculated film stress, E_s is the elastic modulus of the substrate (130 GPa for Si), ν_s is the Poisson's ratio of the substrate (0.28 for Si), d_s and d_f are the thickness of the substrate and film (200 and 0.8 µm respectively), and R is the radius of the measured curvature.

X-Ray Diffraction (XRD) patterns were obtained using CuK_α radiation in θ-2θ mode with a parallel beam set up (Siemens D5000). The patterns were recorded with 2θ ranging from 30 to 50°, with a step size of 0.03°, and 2 s/step acquisition time. The structure of the films was quantified by calculating the texture coefficient T_c, defined as:

$$T_{c(hkl)} = \frac{I_{(hkl)}/I_{r(hkl)}}{n^{-1}\sum I_{(hkl)}/I_{r(hkl)}} \tag{3}$$

where $I_{(hkl)}$ are the intensities from the films, $I_{r(hkl)}$ are the intensities of the reference and n is the number of diffraction peaks considered [25].

To facilitate the phase identification, elemental composition of the films was characterized by energy dispersive X-ray spectroscopy (EDS), using 3 kV acceleration voltage. The Cr Lα (0.573 keV) and N Kα (0.392 keV) lines were used. For the EDS, a Zeiss Merlin with AZtec EDS was employed, equipped with a Schottky FEG and X-Max 80 mm^2 Silicon Drift Detector.

The adhesion and scratch resistance of the coatings were investigated on coated alumina rods. The rods were lapped before deposition, resulting in a smooth surface with randomly distributed pits (S_a value about 20–30 nm and pits up to tens of µm wide and 2–4 µm deep). The surface characteristics remained within these numbers after the deposition.

The films were scratched with a Rockwell C diamond indenter with 200 µm radius, three scratches per sample. The load was increased from 1 to 51 N over 5 mm (10 N/mm) and the scratch speed was 10 mm/min, resulting in a test time of 30 s per scratch. All scratches were investigated with light optical microscopy (LOM) to find the critical load of film failure. A representative selection of the scratches was analysed with scanning electron microscopy (SEM – Zeiss Merlin with Schottky FEG) to identify the failure mechanisms. During the scratching, the normal force, friction force, and acoustic emission were monitored.

Table 1
Varied parameters in reactive sputtering.

Parameter	Variation
N_2 flow	20; 30 sccm
Bias voltage in DCMS	0; −100; −250 V
Bias voltage in HiPIMS	0; −30; −40; −50; −100; −250 V

3. Results and discussion

3.1. Stresses

It was found that increasing the N_2 flow reduces the tensile stresses for both unbiased and −100 V biased DCMS depositions, see Fig. 1. Further, it was found that higher substrate bias does not affect the stress level in the DCMS while in the HiPIMS depositions, the stresses gradually change from tensile to compressive.

All films deposited using DCMS exhibited tensile stresses. The stresses were as high as 400 MPa, when deposited with low N_2 flow and without substrate bias. By increasing the flow of N_2, the stresses were reduced to less than half of the initial value for both biased and unbiased depositions, Fig. 1a. Changes in the substrate bias had very weak effect on the stress level in the DCMS mode especially with low N_2 flow, Fig. 1b. The effect of bias was, however, very strong for HiPIMS. Here, higher bias resulted in very high compressive residual stresses. In fact, coatings deposited by HiPIMS with −100 and −250 V bias

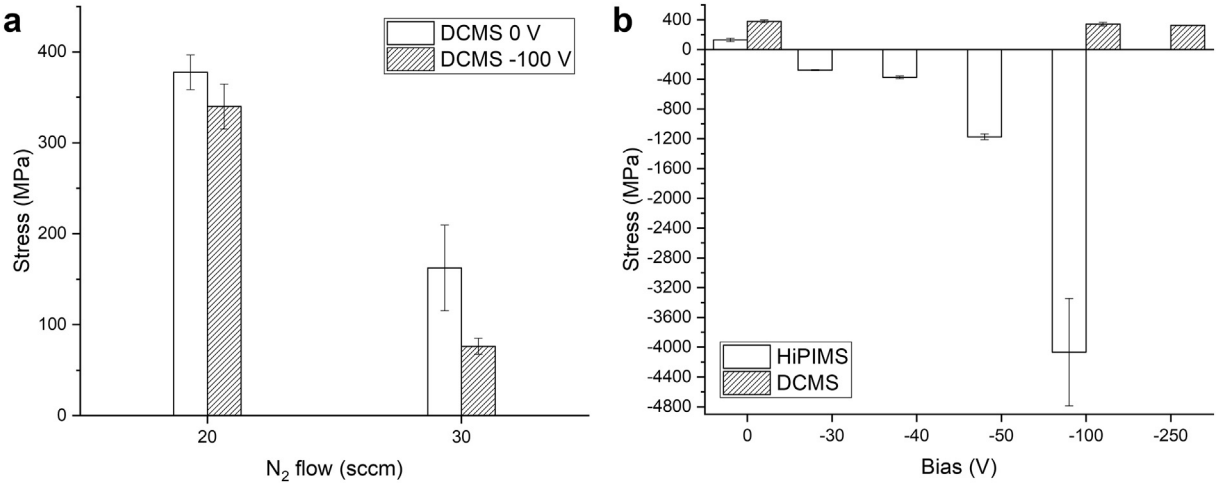

Fig. 1. Residual stresses in the films, calculated from the curvature of the coated thin Si wafers. a) As function of the N_2 flow. b) As function of the DC bias. The film stress of HiPIMS with −100 V bias is calculated from curvature of a thicker Si wafer. Error of the measurement is estimated from the variation in the curvature measured along different axes.

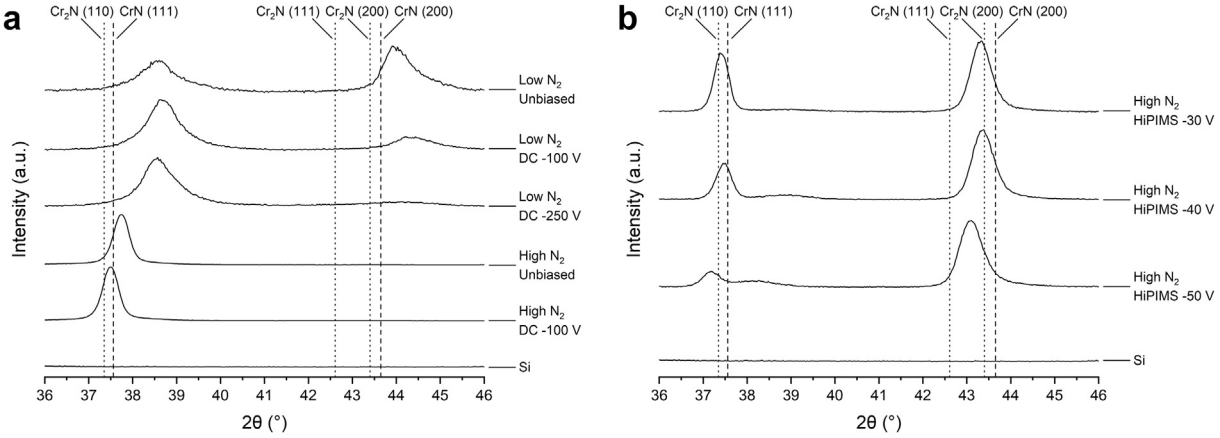

Fig. 2. X-Ray Diffraction results, shift corrected to substrate peaks outside of shown angular range and with intensity range equalised. a) All films have a peak close to CrN (111) and this is more shifted towards higher angles with lower N_2 – corresponding well with the higher tensile stresses in these films. With higher N_2 flow, this peak is the only one remaining and it shifts closer to the reference position. b) The films deposited with HiPIMS all have two peaks close to CrN (111) and CrN (200) and these peaks are shifted towards lower angles for the HiPIMS −50 V film, with the highest compressive stresses.

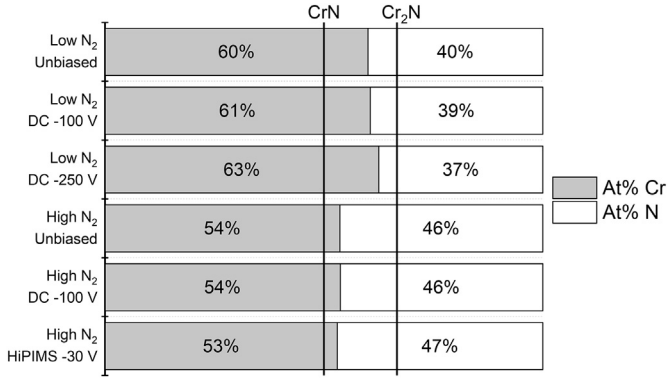

Fig. 3. Elemental composition measured using EDS. The films deposited with low N_2 flow have a lower N content, closer to Cr_2N, compared to the ones deposited with high N_2 flow, closer to CrN.

spontaneously delaminated from most substrates, when removed from the deposition chamber. Therefore, no stress measurements could be made on thin silicon wafers. However, for HiPIMS films deposited with −100 V bias, the stresses were estimated from measurement on a 500 μm thick silicon wafer.

In the absence of thermal stresses, the stress in CrN have been shown to result from two mechanisms, tensile stress generated at the grain boundaries and compressive stress due to ion peening [26]. The observed results for the coatings deposited by DCMS could be explained by a large number of grain boundaries expected for coatings deposited at a low deposition temperature and a lack of ion bombardment. That is consistent with the effect—or rather the lack thereof—of the substrate bias in DCMS. Because of the balanced magnetron source and a long target-to-substrate distance, the ion flux to the substrate is negligible. In the HiPIMS process, on the other hand, the effect of the substrate bias is very strong. This is because a large fraction of the sputtered Cr is ionized and thus accelerated by the applied substrate bias. Very high compressive stresses (reaching −4 GPa) are induced in the film, Fig. 1b. Even moderate substrate bias has a strong influence. It should be noted that the substrate bias was not synchronized with the HiPIMS pulses in this work and therefore implantation of Ar^+ in the afterglow is also expected. This may further increase the compressive stresses [27]. Although the ionized metal flux fraction was not measured in this work, the decreased deposition rate (1.8 times lower in HiPIMS than DCMS) is an indication of Cr ionisation. A large fraction of the created ions is attracted back to the sputtering target and the resulting deposition rate

Table 2
Interpretation of XRD results from variations together with measured residual stresses.

Constant	Variation	Phase and Texture	Residual stresses [MPa]
Low N_2	DCMS: 0 → −250 V	Cr_2N: (110)&(111) → (110)	380 → 320
High N_2	DCMS: 0 → −100 V	CrN(111)	160 → 80
DCMS 0 V	N_2: 20 → 30 sccm	Cr_2N(110)&(111) → CrN(111)	380 → 160
DCMS −100 V	N_2: 20 → 30 sccm	Cr_2N(110) → CrN(111)	340 → 80
High N_2	HiPIMS: 0 → −50 V	CrN: (111) → (111)&(200) → (200)	130 → −280 → −1170

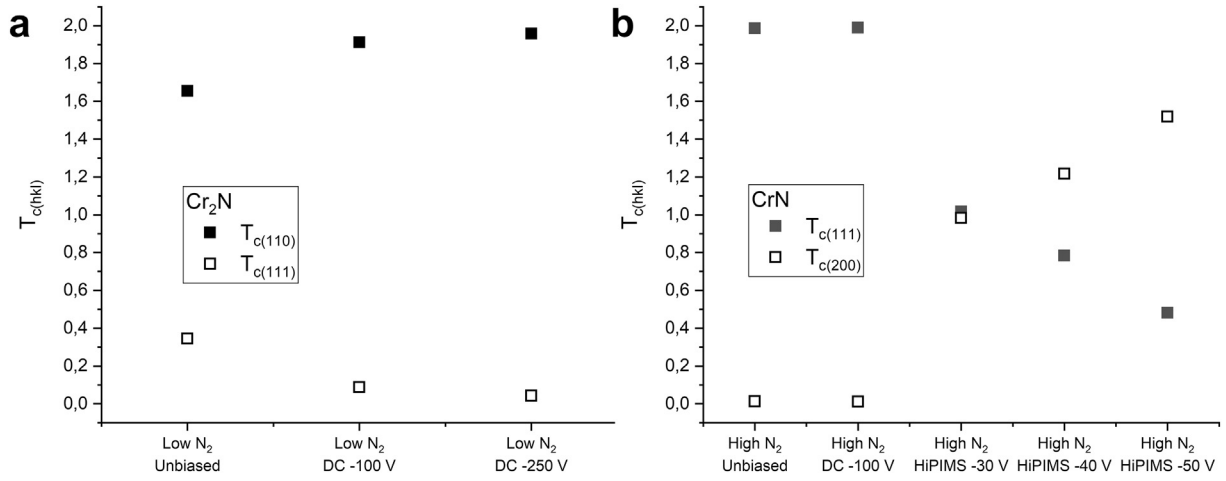

Fig. 4. Texture coefficient $T_{c(hkl)}$, for films with a) low N_2 flow, and b) high N_2 flow. Cr_2N grows preferentially in (110) direction while CrN grows in (111) except when HiPIMS is employed. In the case of HiPIMS, higher bias favours the growth in (200).

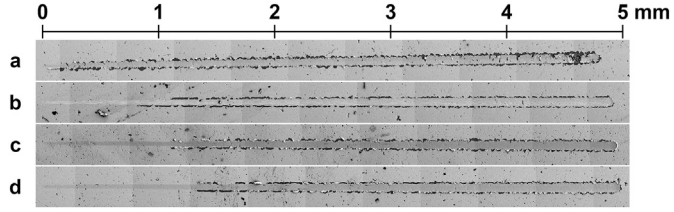

Fig. 5. Examples of appearance of full scratches, scale in mm (load 1–51 N). a) Low N_2 flow, unbiased, 380 MPa, b) High N_2 flow, unbiased, 160 MPa, c) HiPIMS, −30 V, −280 MPa, and d) HiPIMS, −50 V, −1170 MPa. All films were damaged at relatively low loads, resembling recovery spallation. The films with high tensile stresses also cracked across the scratch width, resembling tensile cracking.

is thus reduced [28].

3.2. Structure

The XRD results, Fig. 2, confirmed the influence of the deposition parameters on the film structure. Exact identification of the phases is complicated by the close proximity of the reference positions for CrN (cubic) and Cr_2N (hexagonal) from PDF 01-076-2494 and 00-035-0803, respectively (ICDD, 2019) [29]. The present results can be explained with the help of literature results using similar deposition conditions. The peak shifts due to the residual stresses must be taken into account in such a comparison. In the literature, one of the most substantial effects is that higher N_2 flow favours the formation of CrN over Cr_2N phase [30,31]. Formation of CrN over Cr_2N has also been reported to produce films with lower tensile stresses [6,7]. This agrees well with the measured decrease in tensile stresses with higher N_2 flow, as well as with measured elemental composition, Fig. 3. The XRD results are summarised again in Table 2 to present an overview of all process parameters variations and their effects on the measured residual stresses. The texture coefficient, Fig. 4, shows that with low N_2 flow, the films grow preferentially in the Cr_2N(110) direction. With high N_2 flow, CrN(111) is preferred except for when HiPIMS is employed. Here, higher bias in HiPIMS favours formation of CrN(200) over CrN(111), whereas the opposite has previously been reported [17].

The observed texture evolution in the CrN coatings, Fig. 4, is also

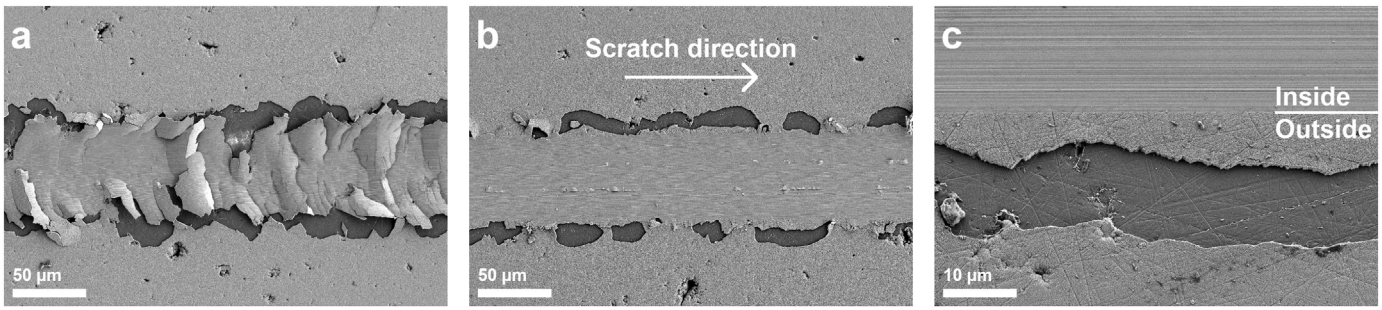

Fig. 6. SEM images illustrating typical failure mechanisms in scratches a) with, and b) without high tensile stresses. If high tensile stresses are present in the coatings, tensile cracks crossing the scratch can be seen. Without high tensile stresses, most of the failure occurs at the scratch border or c) just outside the scratch. This delamination appears to be due to recovery spallation and can be caused by poor adhesion between the coating and the substrate.

related to the ion bombardment. CrN (200) is thermodynamically favoured over the (111) texture. Under kinetically restricted conditions, the low diffusivity (111) oriented grains overgrow the (200) grains and dominate the structure [32]. Due to the low deposition temperature, CrN (111) dominates the coatings deposited by DCMS. The ion assistance in HiPIMS promotes surface diffusion and increasing incident energy of bombarding species, the (200) grain is gradually promoted, Fig. 4b.

3.3. Scratch resistance

The possibility to tune the residual stresses is important in order to optimise the CrN film performance. Scratch testing showed that the first damages occurred at relatively low loads for all films, see Fig. 5. Starting already from relatively low loads, spallation of the entire film thickness down to the substrate was observed.

However, the failure mechanisms resulting from further increasing loads were very different. Films with relatively high residual tensile stresses showed cracking across the width of the scratch track, resembling tensile cracks. The residual stresses combined with the stress from the indenter cause the films to fail completely.

Films with lower tensile stresses or compressive stresses performed much better. The spallation was limited to along the edges of the scratch, resembling recovery spallation [33,34], see Fig. 6. Due to the early initial and continued spallation for all samples, the acoustic emission and CoF showed similar results for all tests and was not possible to use for distinguishing between the samples. The films with low tensile stresses or compressive stresses did not show any signs of failure inside the scratch, even at the highest load. Considering the severity of scratch testing compared to many real applications, this absence of failure inside of the scratch shows the potential of these films.

The results also indicate the importance of adhesion on the scratch performance, since poor adhesion can explain the recovery spallation observed already at low loads. The severity of the damage was reduced when using Ti interlayer in preliminary tests, which might be explained by improved adhesion. In this investigation, the adhesive failure occurs between the interlayer and the substrate. Further optimisation of the surface finish, cleaning process, or the interlayer deposition is therefore expected to improve the overall performance. The qualitative influence of residual stresses, however, will remain the same.

4. Conclusions

We have shown that the residual stresses in CrN_x films can be tailored by varying the deposition conditions. In addition to the traditional parameters, namely substrate bias and N_2 gas flow, the effect of ionisation of the sputtered material in HiPIMS has been investigated. Due to the deposition configuration, the CrN films deposited by DCMC were under tensile residual stresses. Although it was shown possible to reduce the tensile stress magnitude, compressive stresses were achieved only when ionized deposition by HiPIMS was employed. The strong effect of the substrate bias was explained by that it caused high ionisation of the flux of film forming species.

Independent of the stresses, all deposited films showed signs of limited adhesion resulting in recovery spallation right along the scratch border or just outside of the scratch. The response to increasing the scratch test load was highly sensitive to the residual stress level. The films with high tensile stresses cracked across the scratch in a manner resembling tensile cracking, already at low loads, while the films with compressive stresses withstood damage within the scratch up to the highest load.

Even though the loads in scratch testing are high and strongly concentrated, and by this very different from loading in almost any real application, the test is useful for initial evaluation of the coating performance. The results clearly show that it is possible to improve the scratch resistance by tailoring the residual stresses and carefully selecting the interface material.

CRediT authorship contribution statement

Robin Elo: Conceptualization, Investigation, Writing - original draft, Writing - review & editing.**Staffan Jacobson:**Conceptualization.**Tomas Kubart:**Conceptualization, Writing - original draft, Writing - review & editing.

Declaration of competing interest

The authors declare that they have no known competing financial interests or personal relationships that could have appeared to influence the work reported in this paper.

Acknowledgements

Financial support from Swedens Swedish Governmental Agency for Innovation Agency (Vinnova) through the program Materialbaserad konkurrenskraft is gratefully acknowledged.

References

[1] M. Van Stappen, L.M. Stals, M. Kerkhofs, C. Quaeyhaegens, State of the art for the industrial use of ceramic PVD coatings, Surf. Coat. Technol. 74–75 (1995) 629–633, https://doi.org/10.1016/0257-8972(95)08296-4.
[2] E.J. Bienk, H. Reitz, N.J. Mikkelsen, Wear and friction properties of hard PVD coatings, Surf. Coat. Technol. 76–77 (1995) 475–480, https://doi.org/10.1016/0257-8972(95)02498-0.
[3] F. Zhou, C.-M. Suh, S.-S. Kim, R. Murakami, Sliding-wear behavior of TiN- and CrN-coated 2024 aluminum alloy against an Al2O3 ball, Tribol. Lett. 13 (2002) 173–178, https://doi.org/10.1023/A:1020103908345.
[4] A.J. Gant, M.G. Gee, L.P. Orkney, The wear and friction behaviour of engineering coatings in ambient air and dry nitrogen, Wear 271 (2011) 2164–2175, https://doi.org/10.1016/j.wear.2011.02.032.
[5] M.G. Gee, The formation of aluminium hydroxide in the sliding wear of alumina, Wear 153 (1992) 201–227, https://doi.org/10.1016/0043-1648(92)90270-I.
[6] S. Inoue, F. Okada, K. Koterazawa, CrN films deposited by rf reactive sputtering using a plasma emission monitoring control, Vacuum 66 (2002) 227–231, https://doi.org/10.1016/S0042-207X(02)00146-X.
[7] P.H. Mayrhofer, G. Tischler, C. Mitterer, Microstructure and mechanical/thermal properties of Cr–N coatings deposited by reactive unbalanced magnetron sputtering, Surf. Coat. Technol. 142–144 (2001) 78–84, https://doi.org/10.1016/S0257-8972(01)01090-8.
[8] O. Knotek, R. Elsing, G. Krämer, F. Jungblut, On the origin of compressive stress in PVD coatings — an explicative model, Surf. Coat. Technol. 46 (1991) 265–274, https://doi.org/10.1016/0257-8972(91)90169-W.
[9] M. Ahlgren, H. Blomqvist, Influence of bias variation on residual stress and texture in TiAlN PVD coatings, Surf. Coat. Technol. 200 (2005) 157–160, https://doi.org/10.1016/j.surfcoat.2005.02.078.
[10] R. Machunze, A.P. Ehiasarian, F.D. Tichelaar, G.C.A.M. Janssen, Stress and texture in HIPIMS TiN thin films, Thin Solid Films 518 (2009) 1561–1565, https://doi.org/10.1016/j.tsf.2009.09.069.
[11] K. Sarakinos, J. Alami, S. Konstantinidis, High power pulsed magnetron sputtering: a review on scientific and engineering state of the art, Surf. Coat. Technol. 204 (2010) 1661–1684, https://doi.org/10.1016/j.surfcoat.2009.11.013.
[12] J.T. Gudmundsson, N. Brenning, D. Lundin, U. Helmersson, High power impulse magnetron sputtering discharge, J. Vac. Sci. Technol. A 30 (2012) 030801, , https://doi.org/10.1116/1.3691832.
[13] A. Anders, A review comparing cathodic arcs and high power impulse magnetron sputtering (HiPIMS), Surf. Coat. Technol. 257 (2014) 308–325, https://doi.org/10.1016/j.surfcoat.2014.08.043.
[14] D. Lundin, K. Sarakinos, An introduction to thin film processing using high-power impulse magnetron sputtering, J. Mater. Res. 27 (2012) 780–792, https://doi.org/10.1557/jmr.2012.8.
[15] A.P. Ehiasarian, W.-D. Münz, L. Hultman, U. Helmersson, I. Petrov, High power pulsed magnetron sputtered CrNx films, Surf. Coat. Technol. 163–164 (2003) 267–272, https://doi.org/10.1016/S0257-8972(02)00479-6.
[16] G. Greczynski, J. Jensen, L. Hultman, CrNx films prepared by DC magnetron sputtering and high-power pulsed magnetron sputtering: a comparative study, IEEE Trans. Plasma Sci. 38 (2010) 3046–3056, https://doi.org/10.1109/TPS.2010.2071885.
[17] G. Greczynski, J. Jensen, J. Böhlmark, L. Hultman, Microstructure control of CrNx films during high power impulse magnetron sputtering, Surf. Coat. Technol. 205 (2010) 118–130, https://doi.org/10.1016/j.surfcoat.2010.06.016.
[18] F. Ferreira, J.C. Oliveira, A. Cavaleiro, CrN thin films deposited by HiPIMS in DOMS mode, Surf. Coat. Technol. 291 (2016) 365–375, https://doi.org/10.1016/j.surfcoat.2016.02.064.

[19] K. Bobzin, T. Brögelmann, N.C. Kruppe, M. Arghavani, J. Mayer, T.E. Weirich, On the plastic deformation of chromium-based nitride hard coatings deposited by hybrid dcMS/HPPMS: a fundamental study using nanoscratch test, Surf. Coat. Technol. 308 (2016) 298–306, https://doi.org/10.1016/j.surfcoat.2016.05.093.
[20] M.C.R. Guimaraes, B.C.N.M. de Castilho, T. de S. Nossa, P.R.T. Avila, S. Cucatti, F. Alvarez, J.L. Garcia, H.C. Pinto, On the effect of substrate oscillation on CrN coatings deposited by HiPIMS and dcMS, Surf. Coat. Technol. 340 (2018) 112–120, https://doi.org/10.1016/j.surfcoat.2018.02.028.
[21] L.A. Dobrzański, K. Lukaszkowicz, A. Zarychta, Mechanical properties of monolayer coatings deposited by PVD techniques, J. Achiev. Mater. Manuf. Eng. 20 (2007) 423–426.
[22] B. Navinšek, P. Panjan, I. Milošev, Industrial applications of CrN (PVD) coatings, deposited at high and low temperatures, Surf. Coat. Technol. 97 (1997) 182–191, https://doi.org/10.1016/S0257-8972(97)00393-9.
[23] G.G. Stoney, The tension of metallic films deposited by electrolysis, Proc. R. Soc. Lond. Ser. Contain. Pap. Math. Phys. Character. 82 (1909) 172–175, https://doi.org/10.1098/rspa.1909.0021.
[24] J. Laconte, D. Flandre, J.-P. Raskin, Micromachined Thin-film Sensors for SOI-CMOS Co-Integration, Springer US, 2006, https://www.springer.com/gp/book/9780387288420 , Accessed date: 28 May 2019.
[25] R. Romero, D. Leinen, E.A. Dalchiele, J.R. Ramos-Barrado, F. Martín, The effects of zinc acetate and zinc chloride precursors on the preferred crystalline orientation of ZnO and Al-doped ZnO thin films obtained by spray pyrolysis, Thin Solid Films 515 (2006) 1942–1949, https://doi.org/10.1016/j.tsf.2006.07.152.
[26] G.C.a.M. Janssen, F.D. Tichelaar, C.C.G. Visser, Stress gradients in CrN coatings, J. Appl. Phys. 100 (2006) 93512, https://doi.org/10.1063/1.2363818.
[27] G. Greczynski, J. Lu, J. Jensen, S. Bolz, W. Kölker, Ch. Schiffers, O. Lemmer, J.E. Greene, L. Hultman, A review of metal-ion-flux-controlled growth of metastable TiAlN by HIPIMS/DCMS co-sputtering, Surf. Coat. Technol. 257 (2014) 15–25, https://doi.org/10.1016/j.surfcoat.2014.01.055.
[28] N. Brenning, C. Huo, D. Lundin, M.A. Raadu, C. Vitelaru, G.D. Stancu, T. Minea, U. Helmersson, Understanding deposition rate loss in high power impulse magnetron sputtering: I. Ionization-driven electric fields, Plasma Sources Sci. Technol. 21 (2012) 025005, , https://doi.org/10.1088/0963-0252/21/2/025005.
[29] ICDD (2019). PDF-4 + 2019 (Database), edited by Dr. Soorya Kabekkodu, International Centre for Diffraction Data, Newtown Square, PA, USA, (n.d.).
[30] A. Barata, L. Cunha, C. Moura, Characterisation of chromium nitride films produced by PVD techniques, Thin Solid Films 398–399 (2001) 501–506, https://doi.org/10.1016/S0040-6090(01)01498-5.
[31] L. Cunha, M. Andritschky, K. Pischow, Z. Wang, Microstructure of CrN coatings produced by PVD techniques, Thin Solid Films 355–356 (1999) 465–471, https://doi.org/10.1016/S0040-6090(99)00552-0.
[32] R. Daniel, J. Keckes, I. Matko, M. Burghammer, C. Mitterer, Origins of microstructure and stress gradients in nanocrystalline thin films: the role of growth parameters and self-organization, Acta Mater. 61 (2013) 6255–6266, https://doi.org/10.1016/j.actamat.2013.07.009.
[33] S.J. Bull, Failure modes in scratch adhesion testing, Surf. Coat. Technol. 50 (1991) 25–32, https://doi.org/10.1016/0257-8972(91)90188-3.
[34] S.J. Bull, Failure mode maps in the thin film scratch adhesion test, Tribol. Int. 30 (1997) 491–498, https://doi.org/10.1016/S0301-679X(97)00012-1.